Stability Analysis of Visual Servoing with Sliding-mode Estimation and Neural Compensation

Wen Yu

Abstract: In this paper, PD-like visual servoing is modified in two ways: a sliding-mode observer is applied to estimate the joint velocities, and a RBF neural network is used to compensate the unknown gravity and friction. Based on Lyapunov method and input--to-state stability theory, we prove that PD-like visual servoing with the sliding mode observer and the neuro compensator is robust stable when the gain of the PD controller is bigger than the upper bounds of the uncertainties. Several simulations are presented to support the theory results.

Keywords: Neural compensation, sliding-mode, stability, visual servoing.

1. INTRODUCTION

Visual servoing is a flexible and robust control technique of robots using vision in feedback control loops. Visual servoing can be classified into fixed-camera and camera-in-hand configurations. For fixed-camera visual servoing, cameras are in world coordinate frame, they capture images of robots and environment [1]. For the camera-in-hand visual servoing, cameras are mounted on the robot, which can only obtain visual information of the environment [2]. In this paper, we will use the fixed-camera approach. An objective of visual servoing is to move the end effector of robot to desired positions. In the last decade, many visual servoing strategies have been proposed in the literature, see [3] for an overview. Based on the energy-shaping Jacobian transpose, a rigorous analysis of stability for visual-based feedback control is given in [4]. The effects of optical imprecision of cameras on the end effector is analyzed in [1]. [5] uses self-tuning regulator to overcome the off-line calibration problem. [6] and [7] use neural networks to determine the joint angle's velocities for visual servoing. In [8] neural networks are used to compensate the friction in visual servoing. Many visual servoings use PD-like controller as

$$\tau = -K_p\left[x_s - x_s^*\right] - K_d\left[\dot{q} - \dot{q}^*\right], \tag{1}$$

where x_s and x_s^* are the positions of end-effector and target in the images, $\dot{q}$ and $\dot{q}^*$ are real and desired joint velocities, K_p and K_d are positive definite, symmetric and constant matrices, which correspond to proportional and derivative coefficients. Various modifications on PD-like visual servoing have been published, see [1,9,10]. But there are two main weaknesses: (a) The controller requires measurements of joint positions and joint velocities; (b) Due to the existence of friction and gravity, the PD-like visual servoing cannot guarantee zero error of the steady state. The majority velocity sensors are tachometer generators, they provide analog signals that are usually heavily corrupted with noise [11]. A possible solution for steady state error is to add an integrator, named PID visual servoing, but the poles in image axis can cause the closed-loop system unstable [12].

It is very interesting to realize PD-like visual servoing with only joint positions. One possible method is to use velocity observer [13]. Observer-based visual servoing was first presented in [10]. Two kinds of observers can be used, model-based and model-free observers. The model-based observers use complete or partial model information of robots. For example, if the object motion model is assumed to be linear, a Luenberger observer can be applied [14]. A linear observer was presented in [13] by neglecting the nonlinear dynamic of the robot. The model-free observer does not require exact knowledge of robots. The most popular model-free observer is high-gain observer [15]. Neural observer can be regarded as another model-free observer, where robots are estimated by static neural networks [11].

Visual servoing needs transformation from task space into joint space. It requires exact knowledge of the Jacobian matrix. Several efforts have been made to stabilize robots with respect to uncertain Jacobian, where the dimension and joint angles' measurements are not exact [16]. Friction and gravity of robots may

Manuscript received May 30, 2005; revised April 20, 2006; accepted July 4, 2006. Recommended by Editorial Board member Hoon Kang under the direction of Editor Jae-Bok Song.

Wen Yu is with the Departamento de Control Automático, CINVESTAV-IPN, Av.IPN #2508 Mexico D.F., 07360 Mexico, (e-mail: yuw@ctrl.cinvestav.mx).

influence steady and dynamics properties of the closed-loop system. Global asymptotic stability PD control is realized by pulsing gravity compensation in [17]. For robust visual servoing, neural networks can be applied to approximate parts of robot dynamics, for example friction and gravity [8], or the whole dynamics of robots [18]. PD-like visual servoing with sliding-mode observer and neural compensator is presented in [19], where stability analysis is not established. To the best of our knowledge, stability analysis of visual servoing with sliding mode observer and neuro compensator has not yet been established in the literatures.

In this paper, we propose a novel PD-like visual servoing. First, a sliding mode observer is used to estimate joint velocities from joint position measurement, observer-base PD controller is proved to be stable. Then, a RBF neural network is used to estimated friction, gravity and uncertainty of the Jacobian matrix, PD controller with neural compensator is robust stable. The learning algorithm of the neural compensator is obtained from stability analysis of regulation error. By input-to-state stability (ISS) technique and Lyapunov method, we show that the closed-loop system with sliding-mode observer and neuro compensator is robust stable with respect to bounded uncertainties. Some numerical simulations are carried out to validate the theoretical results proposed in this paper.

2. PRELIMINARIES

The main concern of this section is to understand some concepts of robot dynamic, visual servoing, RBF neural networks and input-to-state stability.

2.1. n-links robot dynamic

The dynamics of a serial $n-$ link rigid robot manipulator can be written as [15]

$$M(q)\ \ddot{q}+C(q,\ \dot{q})\ \dot{q}+G(q)+F(\dot{q})=\tau, \qquad (2)$$

where $q\in R^n$ denotes the joints positions, $\dot{q}\in R^n$ denotes the joints velocity, $M(q)\in R^{n\times n}$ is the inertia matrix, $C(q,\ \dot{q})\in R^{n\times n}$ is the centripetal and Coriolis matrix, $G(q)\in R^n$ is the gravity vector, $F(\dot{q})\in R^n$ is a positive definite diagonal matrix of frictional terms, and $\tau\in R^n$ is the input control vector.

This robot model (2) has following structural properties which will be used in the design of velocity observer and nonlinearity compensation [15].

Property 1: The inertia matrix is symmetric and positive definite, i.e.,

$$m_1\|x\|^2\le x^TM(q)x\le m_2\|x\|^2;\forall x\in R^n,$$

where m_1, m_2 are known positive scalar constants, $x\in R^n$ is a vector, $\|\cdot\|$ denotes the euclidean vector norm.

Property 2: The centripetal and Coriolis matrix is skew-symmetric, i.e., satisfies the following relationship:

$$x^T\left[\dot{M}(q)-2C(q,\ \dot{q})\right]\ x=0.$$

2.2. 2-D visual servoing of robot

The relation between the end-effector position $[x\ \ y]^T\in R^2$ and the joint positions $q(t)\in R^n$ is $[x\ \ y]^T=K(q)\ \ [x^*\ \ y^*]^T=K(q^*)$, where $[x^*\ \ y^*]$ and q^* are desired end-effector position and joint position, $K: R^n\to R^2$. The Jacobian matrix $J(\cdot)\in R^{2\times n}$ of the robot is defined as

$$J(q)=\frac{\partial K(q)}{\partial q},\ \ J(q^*)=\frac{\partial K(q^*)}{\partial q^*}. \qquad (3)$$

In order to simplify the proof, in this paper we only discuss regulation problem, i.e., the derivative of the desired position is zero, $\dot{q}^*=0$.

We consider a camera that is vertical to the working plane of the robot manipulator, and the robot's working plane is 2-D, which is shown in Fig. 1.

The image center is in origin of the screen coordinate frame, the camera is rotated about its optical axis by clockwise θ radians, so the rotation matrix is

$$R(\theta)=\begin{bmatrix}\cos\theta & -\sin\theta\\ \sin\theta & \cos\theta\end{bmatrix}.$$

The perspective gain is [14], $h=\dfrac{\lambda}{z-\lambda}$, λ (meter)

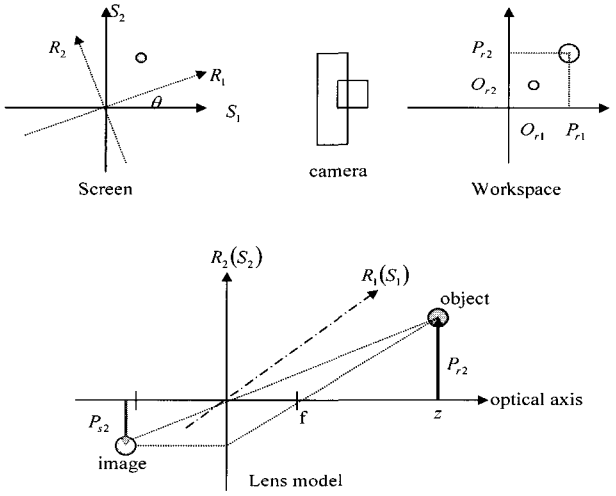

Fig. 1. 2D visual system.

is focal length, z (meter) is distance between camera and robot frame, $z > \lambda$. The scale factor of length units is α (pixels/m). The position of optical axis is $[O_{r1},\ O_{r2}]^T$, a point P in robot coordinate frame is $[p_{r1},\ p_{r2}]^T$, this point in screen coordinate frame is $[p_{s1},\ p_{s2}]^T$, the image center (not in origin of screen coordinate frame) is $[c_x,\ c_y]^T$, so

$$\begin{bmatrix} p_{s1} \\ p_{s2} \end{bmatrix} - \begin{bmatrix} c_x \\ c_y \end{bmatrix} = \alpha h R(\theta) \left(\begin{bmatrix} p_{r1} \\ p_{r2} \end{bmatrix} - \begin{bmatrix} O_{r1} \\ O_{r2} \end{bmatrix} \right), \quad (4)$$

where α is the scale factor of length units. We want to force the end-effector $[x,\ y]^T$ to the target $[x^*,\ y^*]^T$. It is assumed that there exists at least one joint position $q^* \in R^n$ (n-link rigid robot manipulator) such that the robot end-effector is on the target. The image position error $\tilde{x}_s$ is defined as

$$\tilde{x}_s = \begin{bmatrix} x_s^* \\ y_s^* \end{bmatrix} - \begin{bmatrix} x_s \\ y_s \end{bmatrix}, \quad (5)$$

where $(x_s^*,\ y_s^*)$ and $(x_s,\ y_s)$ are the positions of target and end-effector in the images. (5) can be written as

$$\tilde{x}_s = \alpha h R(\theta) \left(\begin{bmatrix} x^* \\ y^* \end{bmatrix} - \begin{bmatrix} x \\ y \end{bmatrix} \right) = \alpha h R(\theta) \left[K(q^*) - K(q) \right]. \quad (6)$$

The velocity property is

$$\frac{d}{dt}\tilde{x}_s = \alpha h R \left[J(q^*)\dot{q}^* - J(q)\dot{q} \right]. \quad (7)$$

A well known PD-like visual servoing control is (for regulation case $\dot{q}^* = 0$)

$$\tau = J^T K_p \tilde{x}_s - K_d \dot{q}, \quad (8)$$

where K_p and K_d are positive definite, symmetric and constant matrices.

2.3. RBF neural networks

Radial Basis Function (RBF) neural networks have recently gained considerable attention. The advantages of the RBF approach, such as the linearity in the parameters and the availability of the fast and efficient training methods, have been noted in several publications [20,21]. RBF neural networks has one hidden layer and a linear output layer. The output of neural networks may be presented as

$$y_j = \sum_{i=1}^{N} w_{i,\,j}\sigma_i(Vx) + b, \quad (9)$$

where N is hidden nodes number, $w_{i,\,j}$ is the weight connecting hidden layer and output layer. x is input vector $x \in R^m$ (m is input node number), $V \in R^{N \times m}$ is the weight matrix in hidden layer, b is the threshold. The significance of the threshold is that the output values have nonzero mean. It can be combined with the first term as $w_{0,\,j} = b$, $\sigma_0(Vx) = 1$, so $y_j = \sum_{i=0}^{N} w_{i,\,j}\sigma_i(Vx)$. $\sigma_i(Vx)$ is radial basis function which we select as Gaussian function $\sigma_j(Vx) = \exp\left\{ \dfrac{\|Vx - c_j\|}{2\rho_j^2} \right\}$, where c_j and ρ_j^2 represent the center and spread of the basis function.

2.4. Input-to-state stability (ISS)

Consider a class of nonlinear systems described by

$$\dot{x}_t = f(x_t,\ u_t), \quad (10)$$

where $x_t \in R^n$ is the state, $u_t \in R^m$ is the input vector, $y_t \in R^m$ is the output vector. $f : R^n \times R^m \to R^n$ is locally Lipschitz. Let us now recall some ISS properties [22].

Definition 1: A system (10) is said to be globally *input-to-state stable* if there exists a $\mathbf{K}$-function $\gamma(s)$ (continuous and strictly increasing $\gamma(0) = 0$) and $\mathbf{KL}$-function $\beta(s,\ t)$ ($\mathbf{K}$-function and for each fixed $s_0 \geq 0$, $\lim_{t \to \infty} \beta(s_0,\ t) = 0$), such that, for each $u_t \in L_\infty$ $\left(\|u(t)\|_\infty < \infty \right)$ and each initial state $x^0 \in R^n$, it holds that $\|x(t,\ x^0,\ u_t)\| \leq \beta\left(\|x^0\|,\ t \right) + \gamma\left(\|u_t\|_\infty \right)$ for each $t \geq 0$.

Definition 2: A smooth function $V : R^n \to R \geq 0$ is called a ISS-Lyapunov function for system (plant) if (a) there exists a $\mathbf{K}_\infty$-function $\alpha_1(\cdot)$ and $\alpha_2(\cdot)$ ($\mathbf{K}$-function and for each fixed $t_0 \geq 0$, $\lim_{s \to \infty} \beta(s,\ t_0) = \infty$) such that

$$\alpha_1(s) \leq V(s) \leq \alpha_2(s), \quad \forall s \in R^n.$$

(b) There exist a $\mathbf{K}_\infty$-function $\alpha_3(\cdot)$ and a $\mathbf{K}$-

function $\alpha_4(\cdot)$ such that

$$\dot{V} \le -\alpha_3(\|x_t\|) + \alpha_4(\|u_t\|).$$

For a nonlinear system, the followings are equivalent [23]: 1) It is input-to-state stable (ISS). 2) It is robustly stable. 3) It admit a smooth ISS-Lyapunov function. If a system is input-to-state stability, the behavior of the system should remain bounded when its inputs are bounded.

3. STABILITY ANALYSIS OF VISUAL SERVOING WITH JOINT VELOCITY OBSERVER

It is well known that one can determine the velocity from the position measurements by differential approximation of the derivative of position

$$\begin{aligned} \dot{x}_1 &= x_2, \\ x_2 &\approx \frac{x_{1,\,t+\delta} - x_{1,\,t}}{\delta}, \quad \delta > 0, \end{aligned} \tag{11}$$

where x_1 is position, x_2 is velocity, δ is a small positive constant, it represents time interval. But the result is not smooth when δ is very small. The most widely used velocity estimator is the high gain observer [24]. But this observer is very sensitive for the output noise. In this paper, we use another model-free observer which can overcome the above shortcomings.

The robot dynamic (2) can be expressed as

$$\dot{x}_t = f(x_t,\ \tau),\ \ y_t = Dx_t, \tag{12}$$

where $x_t = \begin{bmatrix} q \\ \dot{q} \end{bmatrix} \in R^{2n},\ \ x_1 = q,\ \ x_2 = \dot{q},$

$$f(x_t,\ \tau) = \begin{bmatrix} \dot{q} \\ M^{-1}(q)\ \left[\tau - C(q,\ \dot{q})\ \dot{q} - G(q) - F(\dot{q})\right] \end{bmatrix}. \tag{13}$$

If only the joint position is measurable, $D = [I,\ 0]$. (12) can be rewritten as the normal form

$$\begin{aligned} \dot{x}_t &= Ax_t + f_1(x_t,\ u_t), \\ y_t &= Dx_t, \end{aligned} \tag{14}$$

where $f_1(x_t,\ u_t) = f(x_t,\ u_t) - Ax_t$, A is selected such that the pair $(A,\ D)$ is observable.

Let us construct the sliding mode observer as

$$\begin{aligned} \frac{d}{dt}\bar{x}_t &= A\bar{x}_t + S(\bar{x}_t,\ e) - Ke_t, \\ \bar{y}_t &= D\bar{x}_t, \end{aligned} \tag{15}$$

where $\bar{x}_t = \begin{bmatrix} \hat{q} \\ \frac{d}{dt}\hat{q} \end{bmatrix}$, e_t is output error defined as $e_t = \bar{y}_t - y_t = D\bar{\Delta}_t = D(\bar{x}_t - x_t)$, where $\bar{\Delta}_t$ is observer error, $S(\bar{x}_t,\ e_t)$ is selected

$$S(\bar{x}_t,\ e_t) = -\rho\frac{P^{-1}D^T D\bar{\Delta}_t}{\|D\bar{\Delta}_t\|} = -\rho P^{-1}D^T sig(e_t), \tag{16}$$

where $sig(e_t) = \begin{cases} \frac{e_t}{\|e_t\|} & e_t \ne 0 \\ 0 & e_t = 0 \end{cases}$, P is a positive definite matrix, ρ is a positive constant, they will be determined after. Clearly the sliding mode observer (so) is not depended on the nonlinear plant (12), only the output y is needed. This kind of observer is called model-free observer. Although only $\hat{q}$ is needed, we have to use full states to construct the observer, because model-free observers, such as sliding mode and high gain observers, cannot work with partial states. It is different with model-based observer, where reduced-order observer may be applied. The derivative of observer error is

$$\begin{aligned} \frac{d}{dt}\bar{\Delta}_t &= A\bar{\Delta}_t + S(\bar{x}_t,\ e_t) - KD\bar{\Delta}_t - f_1(x_t,\ u_t) \\ &= (A - KD)\ \bar{\Delta}_t + S(\bar{x}_t,\ e_t) - f_1(x_t,\ u_t) \\ &= A_0\bar{\Delta}_t + S(\bar{x}_t,\ e_t) - f_1(x_t,\ u_t), \end{aligned} \tag{17}$$

where $A_0 = A - KD$. Because $(A,\ D)$ is observable there exists K such that A_0 is stable. So the following Lyapunov equation has a positive solution P

$$A_0^T P + PA_0 = -Q,\ \ Q = Q^T > 0 \tag{18}$$

for a positive define matrix Q. By (13) we know $f(x_t,\ u_t)$ is bounded, so following assumption is satisfied.

Assumption 1: $f(x_t,\ u_t) - Ax_t = -P^{-1}D^T h(x_t,\ u_t)$ where $h(x_t,\ u_t)$ is bounded as

$$\|h(x_t,\ u_t)\| \le \bar{h},$$

here $\bar{h}$ is a known positive constant.

Theorem 1: If the observer gain satisfies $\rho > \bar{h}$, the error between the sliding mode observer (12) and the robot (15) is asymptotically stable

$$\lim_{t\to\infty} \bar{\Delta}_t = 0. \tag{19}$$

Proof: Let consider the following Lyapunov function candidate: $V_t = \bar{\Delta}_t^T P\bar{\Delta}_t$. Its derivative is

$$\dot{V}_t = \bar{\Delta}_t^T \left(A_0^T P + P A_0 \right) \bar{\Delta}_t + 2\bar{\Delta}_t^T P \left[S(\bar{x}_t, e_t) - f_1(x_t, u_t) \right].$$

Using Assumption 1

$$f_1(x_t, u_t) = -P^{-1} D^T h(x_t, u_t), \ \| h(x_t, u_t) \| < \rho.$$

Because $\bar{\Delta}_t^T D^T h(x_t, u_t) \le \| D\bar{\Delta}_t \| \ \| h(x_t, u_t) \|$, if we select $S(\bar{x}_t, e_t)$ as (16), we have

$$\begin{aligned} \dot{V}_t &= -\bar{\Delta}_t^T Q \bar{\Delta}_t + 2\bar{\Delta}_t^T D^T h(x_t, u_t) - 2\frac{\bar{\Delta}_t^T D^T D\bar{\Delta}_t}{\| D\bar{\Delta}_t \|} \rho \\ &= -\bar{\Delta}_t^T Q \bar{\Delta}_t + 2\bar{\Delta}_t^T D^T h(x_t, u_t) - 2\| D\bar{\Delta}_t \| \ \rho \\ &\le -\bar{\Delta}_t^T Q \bar{\Delta}_t + 2\| D\bar{\Delta}_t \| \ \left(\| h(x_t, u_t) \| - \rho \right) \le 0. \end{aligned}$$

Since $\dot{V}_t \le 0$, $\bar{\Delta}_t \in L_\infty$. From the error equation (17) we also conclude that $\frac{d}{dt}\bar{\Delta}_t \in L_\infty$. Since $\dot{V}_t \le -\bar{\Delta}_t^T Q \bar{\Delta}_t$ and V_t is bounded process, $\bar{\Delta}_t$ is quadratically integrable and bounded $\Delta_t \in L_2$. Using Barbalat's Lemma we obtain that the observer error $\bar{\Delta}_t$ is asymptotically stable, so $\lim_{t\to\infty} \bar{\Delta}_t = 0$.

The design procedure of sliding-mode observer is to find suitable matrices A, K, Q, and P such that Assumption 1 is satisfied. First we should select a stable matrix A such that (A, C) is observable, now we can find K such that $A_0 = A - KC$ is stable. A stable A_0 can assure (18) has positive solution P, so A1 can be guaranteed.

This sliding mode observer is asymptotically stable, but a robot motion lasts only a finite time, so the observer error cannot be zero in a finite time, we define the estimation error for $\dot{q}$ as

$$\frac{d}{dt}\hat{q} = \dot{q} + \varepsilon.$$

If we choose a large ρ, the convergence speed is very fast such that the observer error is small enough. In the simulation section we will show this observation.

Since $\dot{q}$ is bounded, we can assume ε is bounded for a finite time t, which satisfies following assumption.

Assumption 2: $\varepsilon^T K_d^T \Lambda_\varepsilon K_d \varepsilon \le \bar{\eta}_\varepsilon$,

where Λ_ε is a positive matrix. When the joint velocity $\dot{q}$ is estimated by the sliding-mode observer (15), the observer-based PD-like visual servoing is

$$\tau = J^T K_p \tilde{x}_s - K_d \frac{d}{dt}\hat{q}, \tag{20}$$

where $\dot{\hat{q}} = \bar{x}_2$, $K_p = k_p I$. Following theorem gives a stability property of the observer-based visual servoing.

Theorem 2: If the PD-like visual servoing control (20) is applied to the robot system (2) such that

$$K_d > \Lambda_\varepsilon^{-1} \tag{21}$$

and all other uncertainties such as friction, gravity, image error and the Jacobian matrix error does not exist, the regulation errors $\tilde{x}_s$ and $\dot{q}$ are bounded. The average regulation error $\dot{q}$ converges to

$$\limsup_{T\to\infty} \frac{1}{T} \int_0^T \| \dot{q} \|_{Q_1}^2 \, dt \le \bar{\eta}_\varepsilon, \tag{22}$$

where $Q_1 = K_d - \Lambda_\varepsilon^{-1}$.

Proof: Define Lyapunov function

$$V = \frac{1}{2}\dot{q}^T M \dot{q} + \frac{1}{2\alpha h} \tilde{x}_s^T \left(R^{-1} K_p \right) \tilde{x}_s. \tag{23}$$

Since $K_p = k_p I$, $R^{-1}K_p$ is a symmetric matrix. The time derivative of (23) is

$$\begin{aligned} \dot{V} &= \dot{q}^T M \ddot{q} + \tfrac{1}{2}\dot{q}^T \dot{M} \dot{q} + \tfrac{1}{\alpha h} \dot{x}_S^T \left(R^{-1} K_p \right) \tilde{x}_s \\ &= \tfrac{1}{2}\dot{q}^T \left\{ 2\tau - 2C(q, \dot{q}) \ \dot{q} - 2\left[G(q) + F(\dot{q}) \right] + \dot{M} \dot{q} \right\} \\ &\quad + \tfrac{1}{\alpha h} \dot{x}_S^T \left(R^{-1} K_p \right) \tilde{x}_s. \end{aligned}$$

Using Property 2, $\dot{q}^T \left(\dot{M} - 2C \right) \dot{q} = 0$.

For regulation case $\dot{q}^* = 0$, from (7), $\dot{x}_s = -\alpha h R J \dot{q}$, so

$$\dot{V} = \dot{q}^T \left[\tau - (G + F) - J^T K_p \tilde{x}_s \right].$$

From (20), $\tau = J^T K_p \tilde{x}_s - K_d (\dot{q} + \varepsilon)$.

According to the assumptions of this Theorem, $G + F = 0$

$$\dot{V} = -\dot{q}^T K_d \dot{q} + \dot{q}^T K_d \varepsilon. \tag{24}$$

In view of the matrix inequality,

$$X^T Y + \left(X^T Y \right)^T \le X^T \Lambda^{-1} X + Y^T \Lambda Y, \tag{25}$$

which is valid for any X, $Y \in R^{n\times k}$ and for any positive defined matrix $0 < \Lambda = \Lambda^T \in R^{n\times n}$ [21], $\dot{q}^T K_d \varepsilon$ in (24) can be concluded as

$$\dot{q}^T K_d \varepsilon \le \dot{q}^T \Lambda_\varepsilon^{-1} \dot{q} + \varepsilon^T K_d^T \Lambda_\varepsilon K_d \varepsilon.$$

(24) becomes

$$\dot{V}_1 \le -\dot{q}^T Q_1 \dot{q} + \bar{\eta}_\varepsilon, \tag{26}$$

where $Q_1 = K_d - \Lambda_\varepsilon^{-1}$, from (21) we known $Q_1 > 0$. (24) can be represented as

$$\dot{V} \le -\lambda_{\min}(Q_1) \ \|\dot{q}\|^2 + \varepsilon^T \Lambda_1 \varepsilon \le -\alpha_{\|\dot{q}\|} \|\dot{q}\| + \beta_{\|\varepsilon\|} \|\varepsilon\|,$$

where $\alpha_{\|\dot{q}\|} = \lambda_{\min}(Q_1) \ \|\dot{q}\|$, $\beta_{\|\varepsilon\|} = \lambda_{\max}(\Lambda_1) \ \|\varepsilon\|$, $\Lambda_1 = K_d^T \Lambda_\varepsilon K_d$. So $\alpha_{\|\dot{q}\|}$ and $\beta_{\|\varepsilon\|}$ are $\mathbf{K}_\infty$ functions, V is an ISS-Lyapunov function. Using Theorem 1 and the bound of ε, we conclude that V is bounded. So the regulation error $\tilde{x}_s$ and $\|\dot{q}\|$ are stable.

Integrating (dv1) from 0 up to T yields

$$V_T - V_0 \le -\int_0^T \dot{q}^T Q_1 \dot{q} + \bar{\eta}_\varepsilon T.$$

So

$$\int_0^T \dot{q}^T Q_1 \dot{q} dt \le V_0 - V_T + \bar{\eta}_\varepsilon T \le V_0 + \bar{\eta}_\varepsilon T$$

dividing each term by T, and taking the limit for $T \to \infty$, of these integrals' supreme, we obtain

$$\limsup_{T\to\infty} \frac{1}{T} \int_0^T \|\dot{q}\|_{Q_1}^2 \, dt \le \limsup_{T\to\infty} \left(\frac{V_0}{T} + \bar{\eta}_\varepsilon \right) = \bar{\eta}_\varepsilon,$$

where $\|\dot{q}\|_{Q_1}^2 = \dot{q}^T Q_1 q$, (22) is established.

Remark 1: If we know the gravity G and the friction F, the ideal PD-like visual servoing (8) can be modified as

$$\tau = J^T K_p \tilde{x}_s - K_d \dot{q} + G(q) + F(\dot{q}).$$

The observer-based visual servoing is changed as

$$\tau = J^T K_p \tilde{x}_s - K_d \hat{\dot{q}} + G(q) + F(\dot{q}).$$

The same conclusions as Theorem 3 can be obtained. The regulation error of the PD-like visual servoing is caused by $\bar{\eta}_\varepsilon$ which is the observer uncertainty. Once G, F, and J are not known exactly, the regulation error could be bigger or even leads the whole system to instability. We will discuss this problem in next section.

Remark 2: The Lyapunov function (23) for the stability analysis includes joint velocity $\dot{q}$ and image position $\tilde{x}_s$, Joint position q does not appear in this equation. But from robot inverse kinematics, we can conclude that $q = \xi(x)$ is also bounded.

Remark 3: The results presented in this paper are local, the bound of sliding-mode observer can only be established in a finite time t. We have to estimate the upper bounds of all uncertainties, such that K_d can be decided.

4. STABILITY ANALYSIS OF VISUAL SERVOING WITH NEURAL COMPENSATION

In this section we consider the friction and the gravity are not known absolutely, there exist uncertainties in the Jacobian matrix and the camera model. Let us define $\hat{J}(q)$ as the estimation of $J(q)$, it is assumed that the estimation error is bounded as

Assumption 3: $\eta_J \Lambda_J \eta_J^T \le \bar{\eta}_J$, (27)

here $\bar{\eta}_J$ is upper bound matrix of the uncertainty of Jacobian matrix, $\Lambda_J = \Lambda_J^T > 0$.

The performance of the hand-eye coordination system largely depends on how accurately and quickly the image Jacobean matrix is estimated online. When the camera model is not exactly known, i.e., visual space cannot match the world frame exactly, the incoming images are often corrupted by uncertainties such as changes in illumination, background noise, and camera calibration. For regulation case, (5) becomes

$$\begin{aligned} \tilde{x}_s &= \alpha h R(\theta) \left(\begin{bmatrix} x^* \\ y^* \end{bmatrix} - \begin{bmatrix} x \\ y \end{bmatrix} \right) + e_c(x, \ y) \\ &= \alpha h R(\theta) \ \left[K(q^*) - K(q) \right] + e_c\left[K(q) \right], \end{aligned} \tag{28}$$

where e_c is visual error. The derivative of (28) is

$$\dot{x}_s = -\alpha h R J \dot{q} + e_s J \dot{q}, \tag{29}$$

where e_s is a matrix, which is defined as $e_s = \dot{e}_c$. We assume e_s is bounded as

Assumption 4: $e_s^T \Lambda_s e_s \le \bar{\eta}_s$,

where Λ_s is a positive define matrix. Because x_s and x_s^* are bounded , we have

$$\begin{aligned} &\tilde{x}_s^T K_p \Lambda_J^{-1} K_p \tilde{x}_s \le \eta_1, \\ &\tilde{x}_s^T \left(K_p^T R^{-T} \bar{\eta}_s R^{-1} K_p \right) \ \tilde{x}_s \le \eta_2, \end{aligned} \tag{30}$$

where η_1 and η_2 are positive constants.

The following theorem will prove that the uncertainty

in the estimation of image Jacobean matrix will not destroy the stability. Since we will use neural networks to estimate friction and gravity, the estimation speed will be slowed down, this problem is demonstrated in the simulation.

By neural networks approximation theory [20], the unknown friction and gravity of (2) can be expressed in the form of RBF neural networks (9)

$$G(q)+F(\dot{q})=W^*\sigma(V^*x)+\eta_g, \tag{31}$$

where $x=\left[q^T,\ \dot{q}^T\right]^T$, W^*, V^* are some fixed bounded weights, the $n-$ dimensional vector function $\sigma(\cdot)$ is Gaussian function. η_g is the approximated error, whose magnitude depends on the values of W^* and V^*. According to the Stone-Weierstrass theorem [24], there exists a RBF neural network which can approximate a nonlinear function in any accuracy, so we can assumed that η_g is bounded as

Assumption 5:

$$\eta_g^T\Lambda_g\eta_g\le\overline{\eta}_g, \tag{32}$$

where $\overline{\eta}_g$ is a positive constant. Friction and gravity can be estimated as

$$G(q)+F(\dot{q})\approx\hat{W}_t\ \sigma(\hat{V}_t x),$$

where $\hat{W}_t$ and $\hat{V}_t$ are the weights of the neural networks. It is clear that all Gaussian functions, used in RBF neural networks, satisfy Lipschitz condition

$$\tilde{\sigma}=\sigma(V^{*T}x)-\sigma(\hat{V}_t^Tx)=D_\sigma\tilde{V}_t^Tx+\nu_\sigma, \tag{33}$$

where ν_σ is Taylor approximation error, $\tilde{V}_t=V^*-\hat{V}_t$, $D_\sigma=\frac{\partial\sigma^T(Z)}{\partial Z}|_{Z=\hat{V}_t^Tx}$, which satisfies following assumption

Assumption 6:

$$\nu_\sigma^T\Lambda_\sigma\nu_\sigma\le\overline{\eta}_\sigma, \tag{34}$$

where $\overline{\eta}_\sigma$ is a positive constant. We have following relation

$$\begin{aligned}W^*\sigma(V^*x)-\hat{W}_t\ \sigma(\hat{V}_tx)&=\tilde{W}_t\sigma(V_tx)+W^*\tilde{\sigma}\\&=\tilde{W}_t\sigma(V_tx)+W^*D_\sigma\tilde{V}_tx+\nu_\sigma,\end{aligned} \tag{35}$$

where $\tilde{W}_t=W^*-\hat{W}_t$.

PD-like visual servoing with RBF neural network compensation is

$$\tau=\hat{J}^T\ K_p\tilde{x}_s-K_d\dot{q}+\hat{W}_t\sigma\left(\hat{V}_tx\right), \tag{36}$$

where K_p and K_d are positive definite, symmetric and constant matrices. The following theorem give a stable learning algorithm for PD-like visual servoing with neuro compensation.

Theorem 3: If the proportional gain of the PD visual servoing (36) is selected as

$$K_d>\Lambda_g^{-1}+\Lambda_\sigma^{-1}+\overline{\eta}_J+\overline{J} \tag{37}$$

and the weights of the neuro compensator are updated as

$$\begin{aligned}\tfrac{d}{dt}\hat{W}_t&=-K_w\sigma(V_tx)\dot{q}^T,\\\tfrac{d}{dt}\hat{V}_t&=-K_vxW^*D_\sigma\dot{q}^T,\end{aligned} \tag{38}$$

then the closed-loop system is stable, and the average regulation error $\dot{q}$ converges to

$$\limsup_{T\to\infty}\frac{1}{T}\int_0^T\|\dot{q}\|_{Q_2}^2\,dt\le\overline{\eta}_\sigma+\overline{\eta}_g+\eta_1+\eta_2, \tag{39}$$

where $Q_2=K_d-\left[\Lambda_g^{-1}+\Lambda_\sigma^{-1}+\overline{\eta}_J+\overline{J}\right]$, $\overline{J}\ge J^T\Lambda_s^{-1}J$.

Proof: The proposed Lyapunov function candidate is

$$\begin{aligned}V=&\frac{1}{2}\dot{q}^TM\dot{q}+\frac{1}{2\alpha h}\tilde{x}_s^T\left(R^{-1}K_p\right)\ \tilde{x}_s\\&+\frac{1}{2}tr\left(\tilde{W}_t^TK_w^{-1}\tilde{W}_t\right)+\frac{1}{2}tr\left(\tilde{V}_t^TK_v^{-1}\tilde{V}_t\right),\end{aligned} \tag{40}$$

where K_w and K_v are any positive definite constant matrices. Derivative (40) along the trajectories of (2), yields to:

$$\begin{aligned}\dot{V}=&\dot{q}^TM\ddot{q}+\tfrac{1}{2}\dot{q}^T\dot{M}\dot{q}+\tfrac{1}{\alpha h}\dot{x}_s^T\left(R^{-1}K_p\right)\ \tilde{x}_s\\&+tr\left(\tilde{W}_t^TK_w^{-1}\tfrac{d}{dt}\tilde{W}_t\right)+tr\left(\tilde{V}_t^TK_v^{-1}\tfrac{d}{dt}\tilde{V}_t\right)\\=&\tfrac{1}{2}\dot{q}^T\left\{2\tau-2C(q,\ \dot{q})\ \dot{q}-2\left[G(q)+F(\dot{q})\right]+\dot{M}\dot{q}\right\}\\&+\tfrac{1}{\alpha h}\dot{x}_s^T\left(R^{-1}K_p\right)\tilde{x}_s+tr\left(\tilde{W}_t^TK_w^{-1}\tfrac{d}{dt}\tilde{W}_t\right)+tr\left(\tilde{V}_t^TK_v\tfrac{d}{dt}\tilde{V}_t\right)\end{aligned} \tag{41}$$

Using Property 2 and (29), $\dot{x}_s=-\alpha hRJ\dot{q}+e_sJ\dot{q}$

$$\begin{aligned}\dot{V}=&\dot{q}^T\left[\tau-\left(W^*\sigma(V^*x)+\eta_g\right)-J^TK_p\tilde{x}_s+J^Te_sR^{-1}K_p\tilde{x}_s\right]\\&+tr\left(\tilde{W}_t^TK_w^{-1}\dot{\tilde{W}}_t\right)+tr\left(\tilde{V}_t^TK_v^{-1}\dot{\tilde{V}}_t\right).\end{aligned} \tag{42}$$

Using (34) and (35), we have

$$\begin{aligned}\dot{V}=&-\dot{q}^T\left[\begin{array}{l}\eta_JK_p\tilde{x}_s+J^Te_sR^{-1}K_p\tilde{x}_s+K_d\dot{q}+\tilde{W}_t\sigma(V_tx)\\+W^*D_\sigma\tilde{V}_tx+\nu_\sigma+\eta_g\end{array}\right]\\&+tr\left(\tilde{W}_t^TK_w^{-1}\tfrac{d}{dt}\tilde{W}_t\right)+tr\left(\tilde{V}_t^TK_v^{-1}\tfrac{d}{dt}\tilde{V}_t\right).\end{aligned} \tag{43}$$

By (25),

$$\begin{aligned}\dot{V} =& -\dot{q}^T K_d \dot{q} - \dot{q}^T \eta_J K_p \tilde{x}_s - \dot{q}^T \left[\nu_\sigma + \eta_g \right] \\ &+ \dot{q}^T J^T e_s R^{-1} K_p \tilde{x}_s + tr\left[\left(K_w^{-1} \frac{d}{dt} \tilde{W}_t - \sigma(V_t x) \dot{q}^T \right) \tilde{W} \right] \\ &+ tr\left[\left(K_v^{-1} \frac{d}{dt} \tilde{V} - x W^* D_\sigma \dot{q}^T \right) \tilde{V} \right].\end{aligned}$$

In view of the matrix inequality (25), $\dot{q}^T J^T e_s R^{-1} K_p \tilde{x}_s$, $-\dot{q}^T \left[\nu_\sigma + \eta_g \right]$ and $-\dot{q}^T \eta_J K_p \tilde{x}_s$ in (43) can be estimated as

$$\begin{aligned}-\dot{q}^T \left[\nu_\sigma + \eta_g \right] &\le \dot{q}^T \left(\Lambda_g^{-1} + \Lambda_\sigma^{-1} \right) \dot{q} + \bar{\eta}_g + \bar{\eta}_\sigma \\ -\dot{q}^T \eta_J K_p \tilde{x}_s &\le \dot{q}^T \eta_J \Lambda_J \eta_J^T \dot{q} + \tilde{x}_s^T K_p \Lambda_J^{-1} K_p \tilde{x}_s \\ &\le \dot{q}^T \bar{\eta}_J \dot{q} + \tilde{x}_s^T K_p \Lambda_J^{-1} K_p \tilde{x}_s \\ \dot{q}^T J^T e_s R^{-1} K_p \tilde{x}_s &\le \dot{q}^T J^T \Lambda_s^{-1} J \dot{q} \\ &\quad + \tilde{x}_s^T \left(K_p^T R^{-T} e_s^T \Lambda_s e_s R^{-1} K_p \right) \tilde{x}_s \\ &\le \dot{q}^T \bar{J} \dot{q} + \tilde{x}_s^T \left(K_p^T R^{-T} \bar{\eta}_s R^{-1} K_p \right) \tilde{x}_s,\end{aligned} \tag{44}$$

where $\bar{J} \ge J^T \Lambda_s^{-1} J$. From (38) and (30), we obtain

$$\dot{V} \le -\dot{q}^T Q_2 \dot{q} + \bar{\eta}_\sigma + \bar{\eta}_g + \eta_1 + \eta_2, \tag{45}$$

where $Q_2 = K_d - \left[\Lambda_g^{-1} + \Lambda_\sigma^{-1} + \bar{\eta}_J + \bar{J} \right]$. (45) can be represented as

$$\begin{aligned}\dot{V} &\le -\lambda_{\min}(Q_2) \|\dot{q}\|^2 + \eta_g^T \Lambda_g \eta_g + \nu_\sigma^T \Lambda_\sigma \nu_\sigma + e_s^T \Lambda_a e_s \\ &\le -\alpha_{\|\dot{q}\|} \|\dot{q}\| + \beta_{\|\eta_g\|} \|\eta_g\| + \beta_{\|\nu_\sigma\|} \|\nu_\sigma\| + \beta_{\|e_s\|} \|e_s\|,\end{aligned}$$

where

$$\begin{aligned}&\Lambda_a = K_p \Lambda_J^{-1} K_p + K_p^T R^{-T} \bar{\eta}_s R^{-1} K_p, \\ &\alpha_{\|\bar{x}_2\|} = \lambda_{\min}(Q_2) \|\dot{q}\|, \ \beta_{\|\eta_g\|} = \lambda_{\max}\left(\Lambda_g \right) \|\eta_g\|, \\ &\beta_{\|\nu_\sigma\|} = \lambda_{\max}\left(\Lambda_\sigma \right) \|\nu_\sigma\|, \ \beta_{\|e_s\|} = \lambda_{\max}\left(\Lambda_a \right) \|e_s\|.\end{aligned}$$

So $\beta_{\|e_s\|}$, $\beta_{\|\eta_g\|}$, and $\beta_{\|\nu_\sigma\|}$ are $\mathbf{K}_\infty$ functions, V is an ISS-Lyapunov function. Using Theorem 1 and the bound of η_1, η_2, η_g, and ν_σ, V is bounded. So the regulation error $\tilde{x}_s$ and $\|\dot{q}\|$, the weight $\hat{W}_t$ and $\hat{V}_t$ are stable in the sense of L_∞.

Remark 4: The regulation error converges to the ball radius $\left(\bar{\eta}_J + \bar{\eta}_\sigma + \bar{\eta}_g + \bar{\eta}_s \right)$. Since we do not know those values, it is usual to set these values rather bigger to assure stability. Because the stability condition (37) requires Λ_g^{-1} and Λ_σ^{-1} be smaller, from Assumption 4 and 5 we know this makes $\bar{\eta}_\sigma$ and $\bar{\eta}_g$ bigger. If we set Λ_g^{-1} and Λ_σ^{-1} rather bigger for better regulation performance, then the stability can be crushed. The trade-off between $\bar{\eta}_\sigma$, $\bar{\eta}_g$ and Λ_σ^{-1}, Λ_g^{-1} occurs in the theoretical analysis. For real application, it becomes how to select the gains of PD control. We know bigger PD gains can give better performanc but may destory the stability. It is also correct in (37). When Λ_g^{-1} and Λ_σ^{-1} are bigger (K_d is bigger), $\bar{\eta}_\sigma$ and $\bar{\eta}_g$ becomes smaller. The method to resolve this trade-off is similar as PD control, if we require the control system is more stable, we should choose a smaller K_d, or Λ_g^{-1} and Λ_σ^{-1} are smaller, so $\bar{\eta}_\sigma$ and $\bar{\eta}_g$ are bigger, the regulation performances are sacrificed.

The regulation error is also influenced by the prior known matrices W^*. Theorem 4 shows that W^* does not influence the stability property, and the identification error will be convergence by the algorithm (38). We use the following off-line steps to get the best W^* :

1) W^* is started from any initial value.
2) Update the weights of the neural networks according to (38).
3) If the identification error decreases, W_t becomes the new initial condition, *i.e.*, $W^* = W_t$, goto 2).
4) If the identification error does not decrease, stop off-line identification, now W_t is the final value of W^*.

Remark 5: From the definition of the Lyapunov function (40), we can see that the learning rules (38) minimizes the tacking error $\tilde{x}_s$ and $\dot{q}$. This structure is different from normal neural networks which approximate nonlinear function directly.

If the velocity $\dot{q}$, the friction and the gravity are unknown, PD-like visual servoing is a combination of the velocity estimation (20) and the neuro compensation (36)

$$\tau = \hat{J}^T K_p \tilde{x}_s - K_d \frac{d}{dt} \hat{q} + \hat{W}_t \sigma\left(\hat{V}_t x \right), \tag{46}$$

where $s = \left(x_1^T, \ \hat{x}_2^T \right)^T$. The new PD-like visual servoing is shown in Fig. 2.

We define estimation errors for $\dot{q}$ and $\ddot{q}$ as

$$\frac{d}{dt} \hat{q} = \dot{q} + \varepsilon,$$

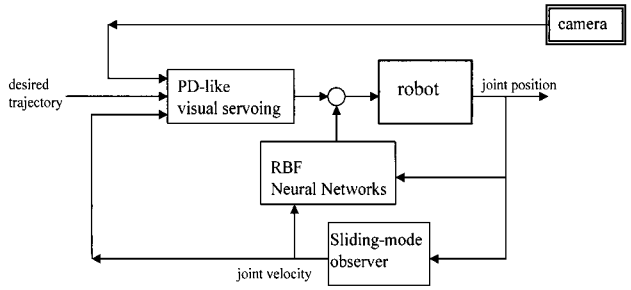

Fig. 2. PD visual servoing.

$$\frac{d^2}{dt^2}\hat{q} = \ddot{q} + \varepsilon_1.$$

ε and ε_1 are bounded, which satisfy following assumptions.

Assumption 7: $\varepsilon^T \Lambda_{\varepsilon_0} \varepsilon \le \bar{\eta}_{\varepsilon_0}$.

Assumption 8: $\varepsilon_1^T \Lambda_{\varepsilon_1} \varepsilon_1 \le \bar{\eta}_{\varepsilon_1}$.

The following theorem gives the stability analysis of the visual servoing (46).

Theorem 4: If the proportional gain of the PD visual servoing (46) is selected as

$$K_d > \Lambda_\varepsilon^{-1} + \Lambda_g^{-1} + \Lambda_\sigma^{-1} + \bar{\eta}_J + \bar{J} + M^T \Lambda_{\varepsilon_1}^{-1} M + \dot{M}^T \Lambda_{\varepsilon_0}^{-1} \dot{M}$$

the weights of the neuro compensator are updated as

$$\begin{aligned} \frac{d}{dt}\hat{W}_t &= -K_w \sigma(V_t s) \frac{d}{dt}\hat{q}^T, \\ \frac{d}{dt}\hat{V}_t &= -K_v s W^* D_\sigma^T \frac{d}{dt}\hat{q}^T, \end{aligned} \tag{47}$$

where $\hat{q}$ is estimated as in (15), then the closed-loop system is stable, and the average regulation error $\dot{\hat{q}}$ converges to

$$\begin{aligned} &\limsup_{T\to\infty} \frac{1}{T} \int_0^T \left\| \frac{d}{dt}\hat{q} \right\|_{Q_3}^2 dt \\ &\le \bar{\eta}_\varepsilon + \bar{\eta}_g + \bar{\eta}_\sigma + \eta_1 + \eta_2 + \bar{\eta}_{\varepsilon_0} + \bar{\eta}_{\varepsilon_1}, \end{aligned} \tag{48}$$

where $Q_3 = K_d - \begin{bmatrix} \Lambda_\varepsilon^{-1} + \Lambda_g^{-1} + \Lambda_\sigma^{-1} + \bar{\eta}_J \\ + \bar{J} + M^T \Lambda_{\varepsilon_1}^{-1} M + \dot{M}^T \Lambda_{\varepsilon_0}^{-1} \dot{M} \end{bmatrix}$.

Proof: Lyapunov function is

$$\begin{aligned} V = &\frac{1}{2}\dot{\hat{q}}^T M \dot{\hat{q}} + \frac{1}{2\alpha h} \tilde{x}_s^T \left(R^{-1} K_p \right) \tilde{x}_s \\ &+ \frac{1}{2} tr\left(\tilde{W}_t^T K_w^{-1} \tilde{W}_t \right) + \frac{1}{2} tr\left(\tilde{V}_t^T K_v^{-1} \tilde{V}_t \right). \end{aligned} \tag{49}$$

The derivative of (49) is

$$\begin{aligned} \dot{V} = &\frac{d}{dt}\hat{q}^T M \frac{d^2}{dt^2}\hat{q} + \frac{1}{2}\frac{d}{dt}\hat{q}^T \dot{M} \frac{d}{dt}\hat{q} + \frac{1}{2\alpha h} \tilde{x}_s^T R^{-1} K_p \tilde{x}_s \\ &+ tr\left(\tilde{W}_t^T K_w^{-1} \frac{d}{dt}\tilde{W}_t \right) + tr\left(\tilde{V}_t^T K_v^{-1} \frac{d}{dt}\tilde{V}_t \right), \end{aligned}$$

here

$$\begin{aligned} 2M \frac{d^2}{dt^2}\hat{q} &= 2M\left(\ddot{q} + \varepsilon_1\right) \\ &= 2\tau - 2C(q,\ \dot{q})\,\dot{q} - 2\left[G(q) + F(\dot{q})\right] + 2M\varepsilon_1 \\ \dot{M} \frac{d}{dt}\hat{q} &= \dot{M}\left(\dot{q} + \varepsilon\right) = \dot{M}\dot{q} + \dot{M}\varepsilon. \end{aligned}$$

Similar as (41),

$$\begin{aligned} \dot{V} = &\frac{d}{dt}\hat{q}^T \begin{bmatrix} \tau - \left(W^* \sigma(V^* x) + \eta_g \right) - J^T K_p \tilde{x}_s \\ + \frac{1}{2\alpha h} \tilde{x}_s^T R^{-1} K_p \tilde{x}_s + M\varepsilon_1 + \dot{M}\varepsilon \end{bmatrix} \\ &+ tr\left(\tilde{W}_t^T K_w^{-1} \frac{d}{dt}\tilde{W}_t \right) + tr\left(\tilde{V}_t^T K_v^{-1} \frac{d}{dt}\tilde{V}_t \right). \end{aligned}$$

By Assumption 7 and 8 $\frac{d}{dt}\hat{q}^T M\varepsilon_1$ and $\frac{d}{dt}\hat{q}^T \dot{M}\varepsilon$ can be estimated as

$$\begin{aligned} \frac{d}{dt}\hat{q}^T M\varepsilon_1 &\le \bar{\eta}_{\varepsilon_1} + \frac{d}{dt}\hat{q}^T M^T \Lambda_{\varepsilon_1}^{-1} M \frac{d}{dt}\hat{q}, \\ \frac{d}{dt}\hat{q}^T \dot{M}\varepsilon &\le \bar{\eta}_{\varepsilon_0} + \frac{d}{dt}\hat{q}^T \dot{M}^T \Lambda_{\varepsilon_0}^{-1} \dot{M} \frac{d}{dt}\hat{q}. \end{aligned}$$

Combine (26) and (45)

$$\dot{V} \le -\frac{d}{dt}\hat{q}^T Q_3 \frac{d}{dt}\hat{q} + \bar{\eta}_\varepsilon + \bar{\eta}_g + \bar{\eta}_\sigma + \eta_1 + \eta_2 + \bar{\eta}_{\varepsilon_0} + \bar{\eta}_{\varepsilon_1},$$

where

$$Q_3 = K_d - \begin{bmatrix} \Lambda_\varepsilon^{-1} + \Lambda_g^{-1} + \Lambda_\sigma^{-1} + \bar{\eta}_J \\ + \bar{J} + M^T \Lambda_{\varepsilon_1}^{-1} M + \dot{M}^T \Lambda_{\varepsilon_0}^{-1} \dot{M} \end{bmatrix}.$$

The other part of the proof is the same as Theorem 4. The following factors affect the PD-like visual servoing (46)

1) $\bar{\eta}_\varepsilon$ and Λ_ε^{-1} correspond to the error of the sliding-mode observer.
2) $\bar{\eta}_J$ and $\tilde{x}_s^T K_p^T \Lambda_J^{-1} K_p \tilde{x}_s$ are caused by Jacobian matrix error.
3) η_1 and η_2 are corresponding to image error.
4) $\bar{\eta}_g$ and Λ_g^{-1} are the estimation error of the friction and gravity.
5) $\bar{\eta}_\sigma$ and Λ_σ^{-1} are Taylor estimated errors of neural networks.

Theorem 1-4 need 8 assumptions on the bounds of the uncertainties Assumption 1-8. These assumptions are not difficult to be satisfied. Any robot dynamic

satisfies Assumption 1. Assumption 2 is a direct conclusion of Theorem 2. Since Jacobian is a matrix function of robot dimension and joint angles, it is bounded, so Assumption 3 is satisfied automatically. The bound of image positions means e_c is bounded, since e_c is smooth $\dot{e}_c = e_s$ is also bounded, so Assumption 4 is right. Assumption 5 is a conclusion of Stone-Weierstrass theorem [24], i.e., if we use RBF neural networks to approximate the continuous function $G(q)+F(\dot{q})$, the approximation error is bounded if the initial condition for the weights are chosen near to their optimal values. The correctness of Assumption 6 is that the active functions of RBF neural networks are Gaussian functions, which satisfy Lipschitz condition. Assumption 7 is the same as Assumption 2. For Assumption 8, ε is estimated error for $\frac{d}{dt}\hat{q}(\bar{x}_2)$ and $\varepsilon_1 = \dot{\varepsilon}$, so ε_1 is corresponding to $\frac{d}{dt}\bar{x}_2$ in (15), since $A\bar{x}_t + S(\bar{x}_t,\ e) - Ke_t$ is bounded, ε_1 is bounded.

Remark 6: Any large gain introduced into a closed-loop system will effect the performance. In this theorem K_d is required to be big enough in order to assure robust stability of visual servoing, but this big K_d will also enlarge noise or disturbances. By classical control theory, too big gain may cause vibration in the tracking process. In next simulation section, we can find this problem.

5. SIMULATION

This paper focuses on theoretical analysis of visual servoing. We will propose several simulations to support the theoretical results discussed in this paper. We believe these simple simulations will not affect the theoretical values of this paper. These theoretical results are helpful for visual servoing experiment in the following items: (a) we can assure that the visual servoing is safe for application; (b) the theorems give rules on how to choose the parameters of PD-like visual servoing (K_d should be bigger than the upper bound of the uncertainty); (c) the theorem give upper bounds of regulation errors.

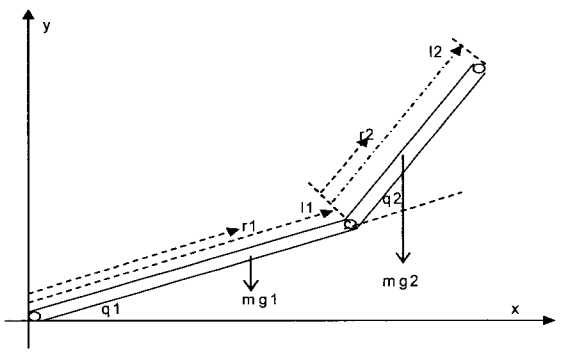

Fig. 3. Two-links robot.

To develop the simulation, a two-link planar robot manipulator is considered. The manipulator is in vertical position, with gravity and friction. A scheme of the two-link robot manipulator is shown in Fig. 3. The elements can be represented as

$$M(q)=\begin{bmatrix} M_{11} & M_{12} \\ M_{21} & M_{22} \end{bmatrix},$$

$$\begin{aligned} M_{11} &= m_1\left(r_1^2/4 + l_1^2/3\right) \\ &\quad + m_2\left(l_1^2 + r_2^2/4 + l_2^2/3 + l_1 l_2\cos q_2\right) \\ &\quad + m_2\left(l_1^2 + 3/4 l_2^2 + l_1 l_2\cos q_2\right), \end{aligned}$$

$$M_{12} = m_2\left(r_2^2/4 + l_2^2/3 + \tfrac{1}{2} l_1 l_2\cos q_2\right) + m_L l_2^2 = M_{21},$$

$$M_{22} = m_2\left(r_2^2/4 + l_2^2/3\right) + m_L l_2^2,$$

$$C(q,\ \dot{q}) = \begin{bmatrix} -V_m\dot{q}_2\sin q_2 & -V_m\sin q_2\left(\dot{q}_1+\dot{q}_2\right) \\ V_m\dot{q}_1\sin q_2 & 0 \end{bmatrix},$$

$$V_m = \left(\tfrac{1}{2} m_2 l_1 l_2 + m_L l_1 l_2\right),$$

$$G(q) = \begin{bmatrix} \left(\tfrac{1}{2} m_1 + m_2\right) g l_1\cos q_1 \\ + \tfrac{1}{2} m_2 g l_2\cos\left(q_1+q_2\right) \\ \tfrac{1}{2} m_2 g l_2\cos\left(q_1+q_2\right) \end{bmatrix},$$

$$F(\dot{q}) = \begin{bmatrix} v_1\dot{q}_1 + k_1 sign(\dot{q}_1) \\ v_2\dot{q}_2 + k_2 sign(\dot{q}_2) \end{bmatrix}.$$

The robot parameters are: $m_1 = 4.8$, $m_2 = 3.3$, $r1 = 0.5$, $r2 = 0.5$, $l_1 = 1$, $l_2 = 1$, $v_1 = 11$, $v_2 = 12$, $k_1 = 0.8$, $k2 = 0.8$, $g = 9.81$. The world (base) frame is

$$\begin{aligned} x &= l_1\cos q_1 + l_2\cos(q_1+q_2), \\ y &= l_1\sin q_1 + l_2\sin(q_1+q_2). \end{aligned}$$

The orientation frame (orientation matrix)

$$\begin{aligned} i_1\cdot i_0 &= \cos\left(q_1+q_2\right), \quad i_1\cdot j_0 = \sin\left(q_1+q_2\right), \\ j_1\cdot i_0 &= -\sin\left(q_1+q_2\right), \quad j_1\cdot j_0 = \cos\left(q_1+q_2\right), \end{aligned}$$

where i, j are standard orthonormal unit vector. Forward kinematic

$$K(q) = \begin{bmatrix} l_1\cos q_1 + l_2\cos q_1\cos q_2 - l_2\sin q_1\sin q_2 \\ l_1\sin q_1 + l_2\cos q_1\sin q_2 + l_2\cos q_2\sin q_1 \end{bmatrix}.$$

Velocity kinematics is

$$\dot{x} = \begin{bmatrix} -l_1\sin q_1 - l_2\sin(q_1+q_2) & -l_2\sin(q_1+q_2) \\ l_1\cos q_1 + l_2\cos(q_1+q_2) & l_2\cos(q_1+q_2) \end{bmatrix}\begin{bmatrix} \dot{q}_1 \\ \dot{q}_2 \end{bmatrix}$$

So Jacobian is

$$J=\begin{bmatrix} -l_1\sin q_1 - l_2\sin(q_1+q_2) & -l_2\sin(q_1+q_2) \\ l_1\cos q_1 + l_2\cos(q_1+q_2) & l_2\cos(q_1+q_2) \end{bmatrix}^T.$$

For the camera we choose

$$R=\begin{bmatrix} 0.7 & -0.72 \\ 0.72 & 0.7 \end{bmatrix}, \quad \alpha=50, \quad z=1, \quad \lambda=0.01.$$

With these parameters, the end-effector in Cartesian space is transformed into visual space by (4). The following simulations are in the visual space. Here we do not consider pixels, by the factor α all the position are in meters. We compare three kinds of visual servoings: normal PD-like visual servoing [1,9], visual servoing with neural compensation [8] and visual servoing with velocity observer and neural compensation proposed in this paper. We consider two different conditions: 1) gravity and friction are known, 2) joint velocities are known. It is well known that normal PD-like visual servoing with both gravity (friction) and joint velocities measurement can reach very good tracking performance, but when gravity (friction) and joint velocities are not available, the new visual servoing presented in this paper will give better performance than the existing approaches. Because without joint velocities, PD-like visual servoing becomes PD-like visual servoing, and without gravity and friction compensation, PD control will destroy zero steady-state error [15].

5.1. Normal visual servoing

We first use a normal PD-like visual servoing (PDn) to regulate the angles of the two-links robot. The desired angles are square waves. If the gravity and friction are unknown, the visual servoing is

$$\tau = J^T K_p \tilde{x}_s - K_d \dot{q}.$$

For this example,

$$\begin{bmatrix} \tau_1 \\ \tau_2 \end{bmatrix} = J^T K_p \begin{bmatrix} x_s^* - x_s \\ y_s^* - y_s \end{bmatrix} - K_d \begin{bmatrix} \dot{q}_1 \\ \dot{q}_2 \end{bmatrix},$$

where $K_p=\begin{bmatrix} 300 & 0 \\ 0 & 300 \end{bmatrix}$, $K_d=\begin{bmatrix} 30 & 0 \\ 0 & 30 \end{bmatrix}$. The regulation results are shown in Fig. 4. There are two problems for this standard PD visual servoing: (a) we have to use angle velocity $[\dot{q}_1,\ \dot{q}_2]$; (b) the steady state error is not zero. If we know the gravity $G(q)$ and the friction $F(\dot{q})$, the visual servoing becomes

$$\tau = J^T K_p \tilde{x}_s - K_d \dot{q} + G(q) + F(\dot{q}).$$

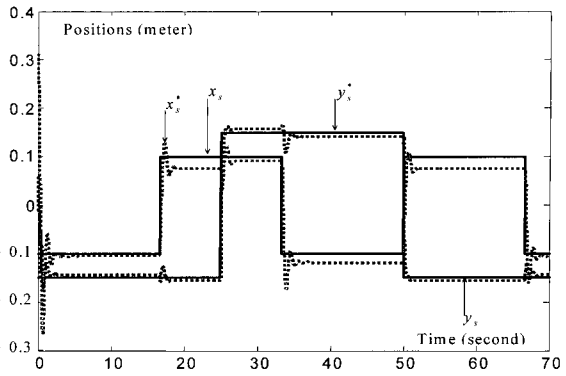

Fig. 4. Normal visual servoing.

The steady-state error is zero.

5.2. Visual servoing with neuro compensation

When the gravity and friction are unknown, they can be uniformly approximated by a radial basis function as in (9), $G(q)+F(\dot{q})\approx\hat{W}_t\sigma(\hat{V}_t x)$. The Gaussian function is

$$\sigma_j(Vx)=\exp\left\{-\frac{\sum_{i=1}^{N}(Vx_i-c_i)^2}{100}\right\},$$

where the spread ρ_l was set to $\sqrt{50}$ and the center c_i is a random number between 0 and 1. The center values of each hidden neuron are initialized randomly. This possibly affects the performance of the system since we cannot assure that the randomization is useful enough to separate each hidden neurons properly. In this simulation, we found that the weight $\hat{W}_t$ affects the performance more than the center c_i. Model complexity is important in the context of system identification, which is corresponded to the number of hidden units of the neuro model. In this simulation we try to test different numbers of hidden nodes, we find that after the hidden nodes is more than 10, the regulation accuracy will not be improved a lot.

The control law is (36)

$$\begin{bmatrix} \tau_1 \\ \tau_2 \end{bmatrix} = J^T K_p \begin{bmatrix} x_s^* - x_s \\ y_s^* - y_s \end{bmatrix} - K_d \begin{bmatrix} \dot{\hat{q}}_1 \\ \dot{\hat{q}}_2 \end{bmatrix} + \hat{W}_t\sigma(\hat{V}_t x)$$

starting with $W^*=0.7$ and $V^*=0.7$ as initial values. Even though some initial weights are needed for the controller to work, no special values are required nor a previous investigation on the robot dynamics for the implementation of this control. Fig. 5 shows the control results. The theoretical result is demonstrated in Theorem 3.

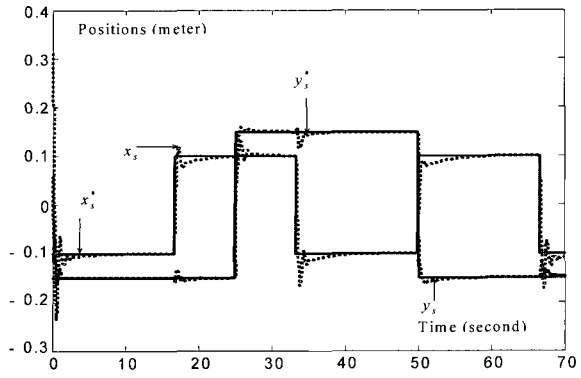

Fig. 5 Neural visual servoing.

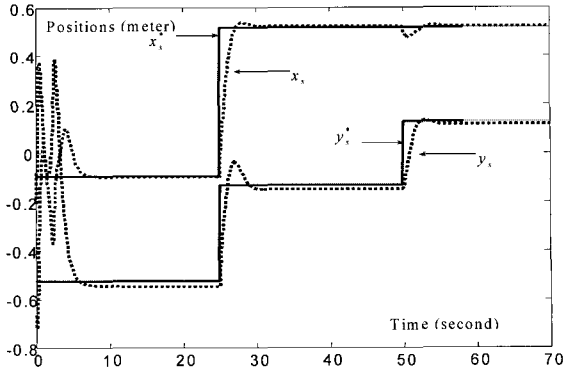

Fig. 6. Observer-based visual servoing.

5.3. Visual servoing with sliding mode observer and neuro compensation

When the joint velocity is not available, we use the sliding-mode observer (14) to obtain $\dot{q} = [\dot{q}_1, \dot{q}_2]^T$. The observer-based PD-like visual servoing (20) is

$$\begin{bmatrix} \tau_1 \\ \tau_2 \end{bmatrix} = J^T K_p \begin{bmatrix} x_s^* - x_s \\ y_s^* - y_s \end{bmatrix} - K_d \begin{bmatrix} \dot{\hat{q}}_1 \\ \dot{\hat{q}}_2 \end{bmatrix}.$$

The regulation results is shown in Fig. 6. Fig. 7 gives the responses of the sliding-mode observer, which is demonstrated in Theorem 1.

We can see that when gravity and friction does not exist, sliding mode observer-based PD visual servoing is effective. Rapid convergence of the observer is essential for the PD-like controller, because it forms part of the feedback. When gravity and friction is presented, we have to use compensation approach to eliminate steady state error, these theoretical results are demonstrated in Theorem 2.

In the worst case, friction and gravity exist and joint velocity is not available. We first use observer to estimate the joint velocity, the PD-like visual servoing without compensation is

$$\begin{bmatrix} \tau_1 \\ \tau_2 \end{bmatrix} = J^T K_p \begin{bmatrix} x_s^* - x_s \\ y_s^* - y_s \end{bmatrix} - K_d \begin{bmatrix} \dot{\hat{q}}_1 \\ \dot{\hat{q}}_2 \end{bmatrix}.$$

The result is shown in Fig. 8. Then we use PD-like visual servoing with neuro compensation

$$\begin{bmatrix} \tau_1 \\ \tau_2 \end{bmatrix} = J^T K_p \begin{bmatrix} x_s^* - x_s \\ y_s^* - y_s \end{bmatrix} - K_d \begin{bmatrix} \dot{\hat{q}}_1 \\ \dot{\hat{q}}_2 \end{bmatrix} + \hat{W}_t \sigma\ (\hat{V}_t x),$$

where K_d should be big enough, such that (see Theorem 4)

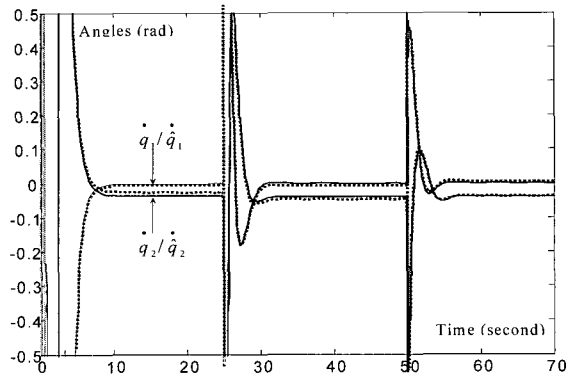

Fig. 7. Sliding mode observer.

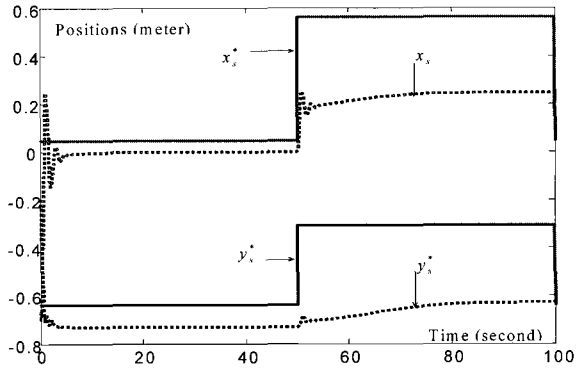

Fig. 8. Unknown gravity and friction.

$$K_d > \Lambda_\varepsilon^{-1} + \Lambda_g^{-1} + \Lambda_\sigma^{-1} + \bar{\eta}_J + \bar{J} + M^T \Lambda_{\varepsilon_1}^{-1} M + \dot{M}^T \Lambda_{\varepsilon_0}^{-1} \dot{M}.$$

We choose the parameters for the upper bounds of the uncertainties as: the sliding-mode observer $\Lambda_\varepsilon^{-1} = diag(1)$, estimation of the friction and gravity $\Lambda_g^{-1} = 5$, Taylor estimation error $\Lambda_\sigma^{-1} = diag(1)$, Jacobian matrix error $\bar{\eta}_J = diag(5)$, $M^T \Lambda_{\varepsilon_1}^{-1} M + \dot{M}^T \Lambda_{\varepsilon_0}^{-1} \dot{M} = 20$. So K_d is selected as $K_d = diag(40)$. We found that when $K_d \geq diag(50)$, the response of the visual servoing becomes vibration. The reason is explained in Remark 6. The result is shown in Fig. 9.

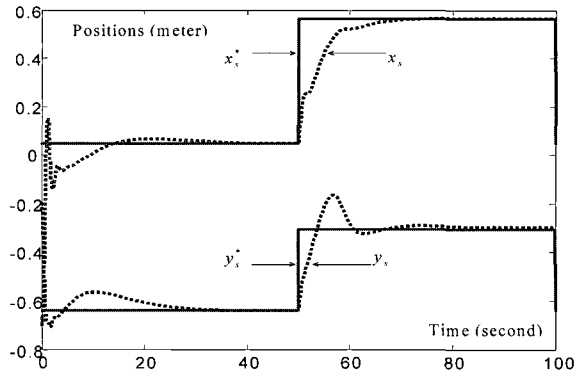

Fig. 9. Neural observer-based.

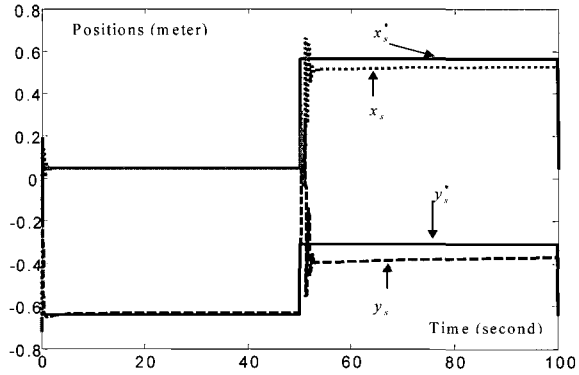

Fig. 10. Neural high-gain observer-based.

We can see that the combination of sliding-mode observer and neuro compensator is a good way to improve the performance of the normal PD-like visual servoing, when gravity, friction and joint velocities are unknown. Compared Fig. 4 with Fig. 6 and Fig. 9, we can see that the response speed is drastic decreased. Because two complete systems: sliding mode observer and neural networks are added in the simple PD controller.

For the same conditions, we use high-gain observer [25] to obtain the join velocities. The high-gain observer is

$$\frac{d}{dt}\hat{x}_1 = \hat{x}_2 + \frac{2.5}{10}(x_1 - \hat{x}_1),$$
$$\frac{d}{dt}\hat{x}_2 = \frac{1.5}{100^2}(x_1 - \hat{x}_1),$$

where $\hat{x} = [\hat{x}_1,\ \hat{x}_1]^T$, $= [\hat{q},\ \frac{d}{dt}\hat{q}]^T$. The visual servoing is shown in Fig. 10. We found that high-gain observer based visual servoing has faster response than sliding mode observer, but the overshot is bigger, and there exists larger steady state error.

6. CONCLUSIONS

In this paper, we have proposed a new PD-like visual servoing based on sliding-mode observer and RBF neural network compensator. The main contribution of this paper is the stability analysis for the closed-loop system by means of Lyapunov and input--to-state stability techniques. Asymptotic stable of sliding-mode observer can be reached provided that the observer gain is bigger than the upper bound of the uncertainty. Robust stabilities of PD-like visual servoing are proved in three cases: PD control with velocity observer, PD control with neural compensator and PD control with velocity observer and neural compensator. Although these three cases require different conditions, they need a common condition: the gain of the PD controller is bigger than the upper bounds of the uncertainties. Future work will be carried out on the improvement of transient properties of the PD-like visual servoing.

REFERENCES

[1] R. Kelly, "Robust asymptotically stable visual servoing of planar robots," *IEEE Trans. on Robotics and Automation*, vol. 12, no. 5, pp. 759-766, 1996.

[2] L. E. Weiss, A. C. Sanderson, and C. P. Neuman, "Dynamic sensor-based control of robots with visual feedback," *IEEE Trans. on Robotics and Automation*, vol. 3, no. 4, pp. 404-417, 1987.

[3] S. Hutchinson, G. D. Hager, and P. I. Corke, "A tutorial on visual servo control," *IEEE Trans. Robotics and Automation*, vol. 12, no. 5, pp. 651-670, 1996.

[4] F. Miyazaki and Y. Masutani, "Robustness of sensory feedback control based on imperfect Jacobian," *Proc. of Robotics Research: 5th Int Symp.*, H. Miurna and S. Arimoto, Eds., Cambridge, MA, pp. 201-208, 1990.

[5] N. P. Papanikolopoulos and P. K. Khosla, "Adaptive robotic visual tracking: Theory and experiments," *IEEE Trans. on Automatic Control*, vol. 38, no. 3, pp. 429-445, 1993.

[6] H. Hashimoto, T. Kubota, M. Sato, and F. Harashima, "Visual control of robotic manipulator based on neural networks," *IEEE Trans. on Industrial Electronics*, vol. 39, no. 6, pp. 490-496, 1992.

[7] V. Santibanez and R. Kelly, "Global asymptotic stability of the PD control with computed feedforward in closed loop with robot manipulators," *Proc. of the 14th IFAC World Congress*, Beijing, pp. 197-203, 1999.

[8] G. Loreto, W. Yu, and R. Garrido, "Stable visual servoing with neural networks compensation," *Proc. of the IEEE International Symposium on Intelligent Control*, Mexico City, Mexico, pp. 183-188, 2001.

[9] B. Espiau, F. Chaumette, and O. Rives, "A new approach to visual servoing in robotics," *IEEE*

Trans. on Robotics and Automation, vol. 8, no. 3, pp. 313-326, 1992.

[10] K. Hashimoto and H. Kimura, "Visual servoing with nonlinear observer," *Proc. of IEEE Int. Conf. Robotics and Automation*, pp. 484-498, 1995.

[11] Y. H. Kim and F. L. Lewis, "Neural network output feedback control of robot manipulators," *IEEE Trans. on Robotics and Automation*, vol. 15, no. 2, pp. 301-309, 1999.

[12] R. Kelly, "A tuning procedure for stable PID control of robot manipulators," *Robotica*, vol. 13, no. 2, pp. 141-148, 1995.

[13] K. Hashimoto and T. Noritsugu, "Visual servoing with linearized observer," *Proc. of IEEE Int. Conf. Robotics and Automation*, pp. 263-268, 1999.

[14] B. K. Ghosh and E. P. Loucks, "A realization theory for perspective systems with application to parametrer estimation problems in machine vision," *IEEE Trans. on Automatic Control*, vol. 41, no. 12, pp. 1706-1722, 1996.

[15] M. Spong and M. Vidyasagar, *Robot Dynamics and Control*, New York, Wiley, 1989.

[16] C. C. Cheah, K. Lee, S. Kawamura, and S. Arimoto, "Asympototic stability of robot control with approximate Jacobian matrix and its application to visual servoing," *Proc. of the 40th Conference on Decision and Control*, Orlando, USA, 2001.

[17] M. Takegaki and S. Arimoto, "A new feedback method for dynamic control of manipulator," *ASME Journal of Dynamic Systems, Measurement, and Control*, vol. 103, pp. 119-125, 1981.

[18] F. L. Lewis and T. Parisini, "Neural network feedback control with guaranteed stability," *Int. J. Control*, vol. 70, no. 3, pp. 337-339, 1998.

[19] W. Yu and X. Li, "Visual servoing with velocity observer and neural compensation," *Proc. of IEEE International Symposium on Intelligent Control*, Taipei, Taiwan, pp. 454-459, 2004.

[20] S. Haykin, *Neural Networks: A Comprehensive Foundation*, Macmillan College Publ. Co., New York, 1994.

[21] W. Yu and X. Li, "Some new results on system identification with dynamic neural networks," *IEEE Trans. on Neural Networks*, vol. 12, no. 2, pp. 412-417, 2001.

[22] C. I. Byrnes, A. Isidori, and J. C. Willems, "Passivity feedback equivalence and the global stabilization of minimum phase nonlinear systems," *IEEE Trans. on Automatic Control*, vol. 36, no. 11, pp. 1228-1240, 1991.

[23] E. D. Sontag and Y. Wang, "On characterization of the input-to-state stability property," *System & Control Letters*, vol. 24, pp. 351-359, 1995.

[24] G. Cybenko, "Approximation by superposition of sigmoidal activation function," *Math. Control, Sig Syst*, vol. 2, pp. 303-314, 1989.

[25] H. K. Khalil, *Nonlinear Systems*, 3rd Edition, Prentice-Hall, NJ, 1999.

Wen Yu received the B.S. degree from Tsinghua University, Beijing, China in 1990 and the M.S. and Ph.D. degrees, both in Electrical Engineering, from Northeastern University, Shenyang, China, in 1992 and 1995, respectively. From 1995 to 1996, he served as a Lecture in the Department of Automatic Control at Northeastern University, Shenyang, China. In 1996, he joined CINVESTAV-IPN, México, where he is a Professor in the Departamento de Control Automático. He has held a research position with the Instituto Mexicano del Petróleo, from December 2002 to November 2003. He is currently an Associate Editor of Neurocomputing, and International Journal of Modelling, Identification and Control. He is a Senior Member of IEEE. His research interests include adaptive control, neural networks, and fuzzy Control.